Cancer Cell
Article

Haploinsufficiency of *SAMD9L*, an Endosome Fusion Facilitator, Causes Myeloid Malignancies in Mice Mimicking Human Diseases with Monosomy 7

Akiko Nagamachi,[1,6] Hirotaka Matsui,[1,6] Hiroya Asou,[1] Yuko Ozaki,[1] Daisuke Aki,[1] Akinori Kanai,[1] Keiyo Takubo,[3] Toshio Suda,[3] Takuro Nakamura,[4] Linda Wolff,[5] Hiroaki Honda,[2,*] and Toshiya Inaba[1,*]
[1]Department of Molecular Oncology and Leukemia Program Project
[2]Department of Disease Model, Research Institute for Radiation Biology and Medicine
Hiroshima University, 1-2-3 Kasumi, Minami-ku, Hiroshima 734-8553, Japan
[3]Department of Cell Differentiation, The Sakaguchi Laboratory of Developmental Biology, Keio University School of Medicine, Shinjuku-ku, Tokyo 160-8582, Japan
[4]Division of Carcinogenesis, Cancer Institute, Japanese Foundation for Cancer Research, Tokyo 135-0063, Japan
[5]Leukemogenosis Section, Laboratory of Cellular Oncology, National Cancer Institute, NIH, Bethesda, MD 20892-4255, USA
[6]These authors contributed equally to this work
*Correspondence: hhonda@hiroshima-u.ac.jp (H.H.), tinaba@hiroshima-u.ac.jp (T.I.)
http://dx.doi.org/10.1016/j.ccr.2013.08.011

SUMMARY

Monosomy 7 and interstitial deletion of 7q (−7/7q−) are well-recognized nonrandom chromosomal abnormalities frequently found among patients with myelodysplastic syndromes (MDSs) and myeloid leukemias. We previously identified candidate myeloid tumor suppressor genes (*SAMD9*, *SAMD9-like* = *SAMD9L*, and *Miki*) in the 7q21.3 subband. We established *SAMD9L*-deficient mice and found that *SAMD9L*$^{+/-}$ mice as well as *SAMD9L*$^{-/-}$ mice develop myeloid diseases resembling human diseases associated with −7/7q−. *SAMD9L*-deficient hematopoietic stem cells showed enhanced colony formation potential and in vivo reconstitution ability. SAMD9L localizes in early endosomes. *SAMD9L*-deficient cells showed delays in homotypic endosome fusion, resulting in persistence of ligand-bound cytokine receptors. These findings suggest that haploinsufficiency of *SAMD9L* and/or *SAMD9* gene(s) contributes to myeloid transformation.

INTRODUCTION

The first report of monosomy 7 in patients with myeloid malignancies was published in 1964, soon after the discovery of the Philadelphia chromosome in 1960, that described the deletion of a C group chromosome in three patients with refractory anemia (myelodysplastic syndrome [MDS] by current criteria) that subsequently developed acute myelogenous leukemia (AML) (E.J. Freireich et al., 1964, Clin. Res., abstract). Since then, −7/7q− has been established as the most representative chromosomal abnormality in a wide variety of myeloid malignancies (10%–20%), including sporadic MDS in the elderly as the sole anomaly, secondary AML in young patients, and AML carrying leukemogenic chimeras as an additional chromosome abnormality (Brunning et al., 2008; Johnson and Cotter, 1997). Tremendous efforts have been made for decades to isolate the responsible genes in 7q. Recent studies indicate that the most frequent deletions among patients with MDS/AML occur within two broad regions with ambiguous borders near bands 7q22 and 7q34 (Jerez et al., 2012).

We recently identified a common microdeletion cluster in subband 7q21.3 in patients with juvenile myelomonocytic leukemia using microarray comparative genomic hybridization (mCGH) (Asou et al., 2009). This cluster contains three poorly

Significance

Chromosome loss may contribute to oncogenesis through mechanisms different from those caused by small deletions, which typically eliminate the function of one tumor suppressor gene by the deletion of one allele and a mutation in the other. In this report, we investigate two related genes, *SAMD9* and *SAMD9L*, as candidate-responsible genes for monosomy 7. Taking advantage that mouse lacks *SAMD9* gene, we established *SAMD9L*-deficient mice and found that *SAMD9L*$^{+/-}$ mice develop myeloid diseases strikingly resembling human diseases associated with −7/7q−. Because haploinsufficiency of an adjacent gene *Miki* contributes to the development of MDS through mitotic/nuclear abnormalities, our studies exemplify a mechanism for how large chromosome deletion can contribute to oncogenesis via haploinsufficiency of multiple responsible genes.

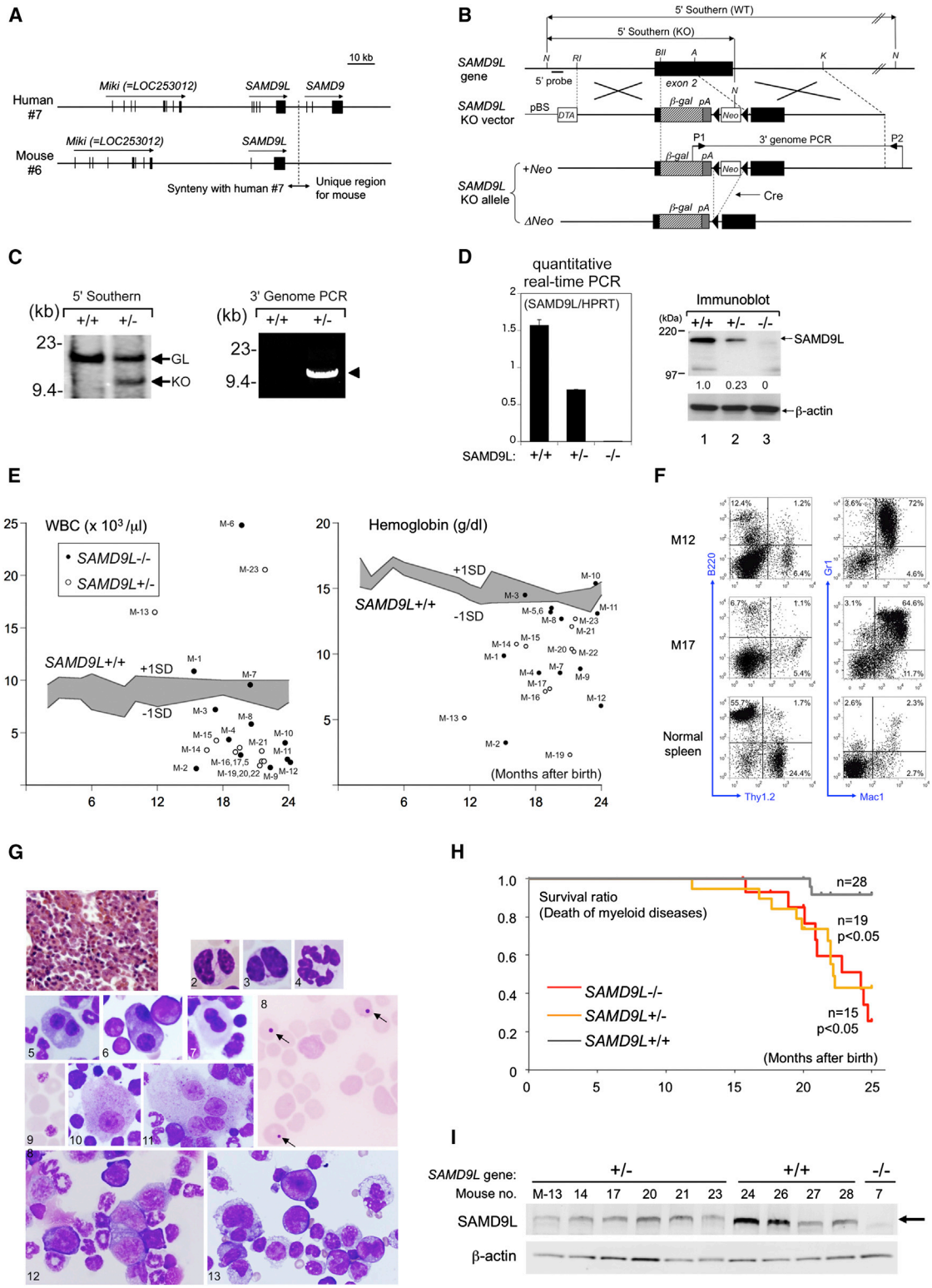

Figure 1. Development of Myeloid Dysplasia in *SAMD9L*-Deficient Mice

(A) Syntenic homology of the *SAMD9L* gene between humans and mice is presented. In humans, two related genes, *SAMD9* and *SAMD9L*, exist in tandem, whereas mice have only *SAMD9L*.

(B) Targeting strategy is illustrated. Part of the coding region of exon 2 is deleted and replaced by the *β-galactosidase* (*β-gal*) gene with the *polyA* (*pA*) and *floxed Neo*-resistance genes for removal of the *Neo*-resistance cassette by Cre recombinase. The positions of the 5′ probe for Southern blot and P1 and P2 primers for genomic PCR are shown. Restriction sites are *N* (NcoI), *RI* (EcoRI), *BII* (BglII), *A* (ApaI), and *K* (KpnI).

(legend continued on next page)

characterized genes: *sterile α motif* (*SAM*) *domain*-9 (*SAMD9*), *SAMD9L*, and *Miki* (*LOC253012*). Although mutations have rarely been seen in these genes, the genes reside proximal to the 7q22 band that is deleted in single copy in nearly 25% of patients with AML and MDS (Asou et al., 2009). We also found that Miki, a centrosomal protein that promotes alignment of chromosomes at metaphase, is a candidate gene responsible for mitotic/nuclear abnormalities routinely observed in patients with MDS (Ozaki et al., 2012).

The human *SAMD9* (*hSAMD9*) and *hSAMD9L* genes share a common gene structure and encode proteins with 60% amino acid identity. A common ancestral gene of *SAMD9/SAMD9L* is found in fish, frogs, and birds and shares roughly equal amino acid identity with both genes. Most mammals including rats have both *SAMD9* and *SAMD9L*. However, mice have only *SAMD9L*, and cows encode only an *SAMD9* homolog (Li et al., 2007), suggesting that SAMD9 and SAMD9L at least partially complement each other's functions. In humans, deleterious mutations in the *SAMD9* gene are known to cause normophosphatemic familial tumoral carcinosis (NFTC) (Topaz et al., 2006), a rare autosomal recessive disease. Because NFTC is characterized by abnormal inflammation of the skin and gingiva that is induced by excessive signaling via tumor necrosis factor α and/or interferon-γ pathways, it has been suggested that SAMD9 suppresses these inflammatory pathways (Chefetz et al., 2008). In this study, we establish *SAMD9L*-deficient mice to study possible roles of SAMD9L in the development of myeloid malignancies and elucidate its biological function.

RESULTS

SAMD9L-Deficient Mice Developed Myeloid Disorders

Mouse synteny for human chromosome subband 7q21.3 ends at the *SAMD9L* gene, and no *SAMD9* gene is present in the mouse genome (Figure 1A). We designed an *SAMD9L* knockout (KO) vector in which the central portion of exon 2 (encoding the entire SAMD9L protein) was removed and replaced with the β-*galactosidase* cDNA and an SV40 *polyA* signal, followed by a *floxed neomycin*-resistance cassette (Figure 1B). Recombinant embryonic stem cell clones (Figure 1C) were used to create $SAMD9L^{+/-}$ and $SAMD9L^{-/-}$ mice.

SAMD9L mRNA was expressed ubiquitously in mice with the highest expression in the kidney (Jiang et al., 2011). Quantitative real-time PCR revealed that the level of SAMD9L mRNA expression in the kidney of $SAMD9L^{+/-}$ mice was 45% of that in WT mice, whereas the protein expression level decreased 4-fold on immunoblots (Figure 1D).

$SAMD9L^{-/-}$ (n = 15), $SAMD9L^{+/-}$ (n = 19), and $SAMD9L^{+/+}$ (n = 28) littermates were observed regularly for signs of illness, including routine examination of peripheral blood. Among 28 $SAMD9L^{+/+}$ mice, all but 2 maintained consistent WBC counts and hemoglobin (Hb) levels throughout the 24-month observation period (Figure 1E, shaded areas). Five of the $SAMD9L^{+/+}$ mice died during the observation period (Table S1 available online).

Among 34 $SAMD9L^{+/-}$ and $SAMD9L^{-/-}$ mice, all but 1 (M-13) showed normal WBC counts and Hb levels until the age of 12 months; thereafter, 12 mice (M-2, M-5, M-9, M-11, M-12, M-14, M-16, M-17, M-19, M-20, M-21, and M-22) developed neutropenia (WBC <4,000/μl), 3 mice (M-1, M-4, and M-7) suffered from anemia (Hb <10 g/dl) with normal WBC counts, whereas 3 mice (M-6, M-13, and M-23) showed an apparent WBC increase (>15,000/μl) (Figure 1E). Of 23 mice associated with those abnormal hematological findings, 18 had markedly enlarged spleen (Table S1), in which Gr1/Mac1-positive myeloid cells were proliferated (Figure 1F). All 15 mice developing cytopenia showed bone marrow (BM) with normal or even increased cellularity (Figure 1G, panel 1), and myelodysplasia included Pseudo-Pelger-Huet anomaly (panels 2 and 3), hypersegmented neutrophils (panel 4), erythroblasts with abnormal nuclei (panels 5–7), Howell-Jolly body, polychromasia, anisopoikilocytosis (panel 8), giant platelets (panel 9), and megakaryocytes with round shape nuclei (panels 10 and 11). BM frequently showed erythroid and/or myeloid maturation arrest (Figure 1G, panels 12 and 13). Based on Bethesda proposals for classification of nonlymphoid hematopoietic neoplasms in mice (Kogan et al., 2002), the types and frequencies of myeloid diseases included myeloid dysplasia (8 of 15 $SAMD9L^{-/-}$; 8 of 19 $SAMD9L^{+/-}$), myeloid leukemia (1 of 15 $SAMD9L^{-/-}$; 1 of 19 $SAMD9L^{+/-}$), and myeloproliferative disease (1 of 19 $SAMD9L^{+/-}$).

SAMD9L-deficient mice died of myeloid disease (Figure 1H; Table S1) at significantly higher frequency than $SAMD9L^{+/+}$ mice ($p < 0.05$, log rank test). $SAMD9L^{+/-}$ mice that developed myeloid diseases still expressed SAMD9L protein (Figure 1I), and no mutations were detected in the coding regions of the *SAMD9L* gene or mRNA.

MOL4070A Infection Accelerated Disease Latency and Frequency

MOL4070A retrovirus (Wolff et al., 2003), a derivative of Moloney murine leukemia virus, induces myeloid malignancies in

(C) 5′ Southern blot and 3′ genomic PCR to detect homologous recombination are shown. Germline (GL) and KO allele-derived bands are indicated by arrows (left panel), and the recombination-specific PCR product is indicated by the arrowhead (right).
(D) SAMD9L transcripts analyzed by quantitative real-time PCR and normalized by HPRT (left) are shown. Immunoblot analysis of kidney extract used SAMD9L (top) or β-actin (bottom) antibody (right). *SAMD9L* genotypes are indicated below (left) or above (right). The relative expression ratio of SAMD9L to β-actin is indicated between the two panels. Error bars, SD.
(E) Peripheral WBC count (left) or Hb level (right) is presented. Shaded areas indicate the range of values from −1 to +1 SD in $SAMD9L^{+/+}$ mice. Closed circles indicate $SAMD9L^{-/-}$ mice; open circles represent $SAMD9L^{+/-}$ mice.
(F) Flow cytometric analysis of splenic cells is shown.
(G) Hematoxylin-eosin staining of formalin-fixed BM (panel 1), Giemsa-stained peripheral blood (panels 2–4, 8, and 9), and BM smears (panels 5–7 and 10–13) from *SAMD9L*-deficient mice that developed MDS is shown. Arrows indicate Howell-Jolly bodies (panel 8). Scale bars, 5 μm.
(H) Myeloid disease-free survival curves are illustrated. Data from mice that died of causes other than myeloid malignancies are censored.
(I) Immunoblot analysis of mouse splenic cell extracts used SAMD9L (top) or β-actin (bottom) antibody. *SAMD9L* genotypes are indicated above. The arrow indicates the position of SAMD9L.
See also Table S1.

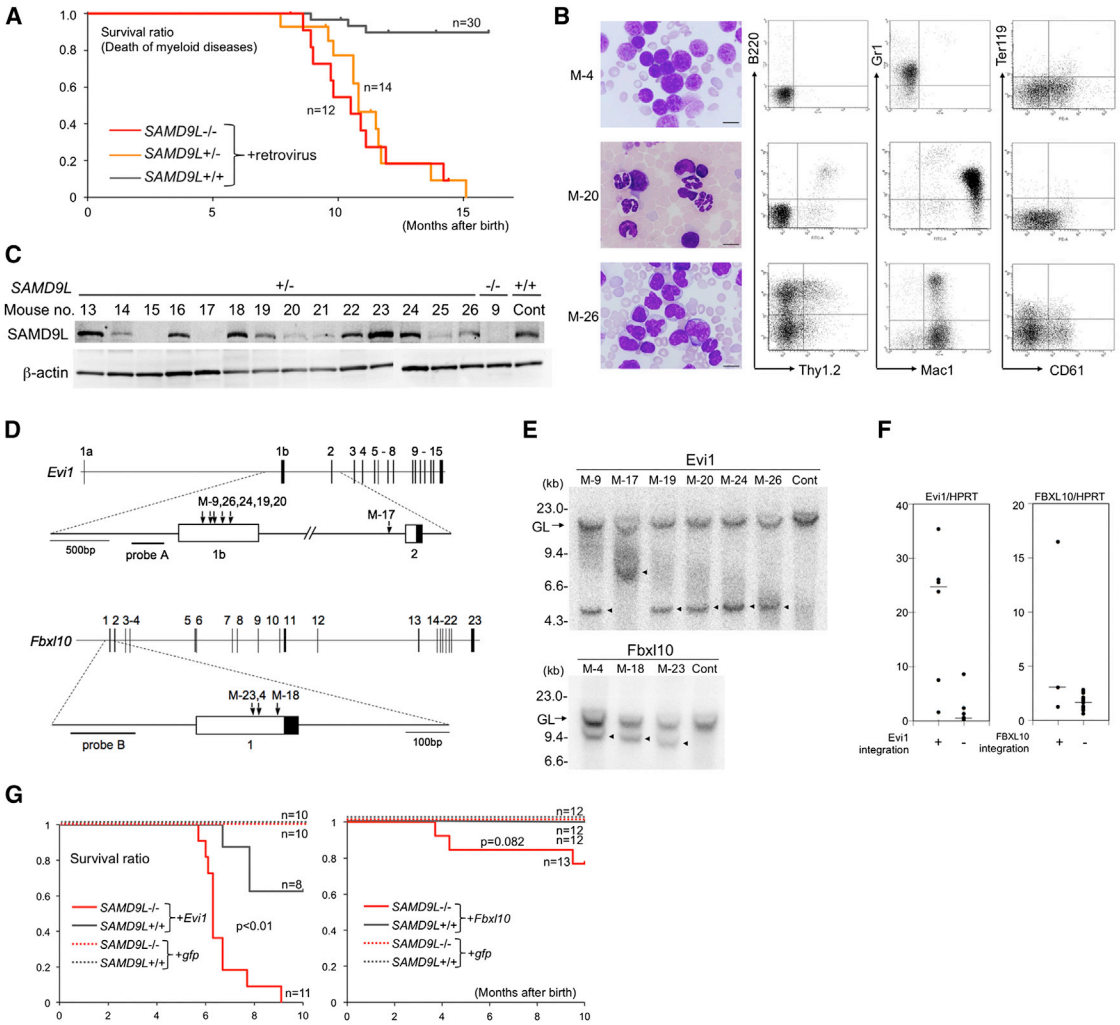

Figure 2. *SAMD9L* Deficiency Predisposes Mice to Myeloid Malignancies

(A) Myeloid disease-free survival curves of mice infected with MOL4070A retrovirus are presented. Data from mice that died of causes other than myeloid malignancies are censored.

(B) Representative phenotypes of myeloid leukemia are shown. Wright-Giemsa staining of peripheral blood smears and results of flow cytometric analysis of splenic cells are shown. Scale bars, 10 μm.

(C) Immunoblot analysis of extracts from splenic cells used SAMD9L (top) or β-actin (bottom) antibody. Mouse number and genotype are indicated above.

(D) Schematic illustration of the *Evi1* (top) and *Fbxl10* (bottom) genes identified as CISs is shown. Vertical arrows indicate viral integration sites.

(E) Southern blot analysis to detect retroviral integration is presented. Germline (GL) bands (arrows) and rearranged bands (arrowheads) are indicated.

(F) *Evi1* (left) and *Fbxl10* (right) transcripts analyzed by quantitative real-time PCR and normalized to the level of HPRT transcripts in splenic cells from mice with or without integration of the indicated gene are shown. Horizontal short lines indicate median values.

(G) Survival curves of lethally irradiated mice that had been transfused with BM cells from *SAMD9L*$^{-/-}$ or *SAMD9L*$^{+/+}$ mice infected with either *Evi1*- or control (*GFP*)-expressing retrovirus (left panel) or with either *Fbxl10*- or control (*GFP*)-expressing retrovirus (right panel) are illustrated.

See also Tables S2–S4.

mice harboring a propensity for myeloid diseases (Castilla et al., 2004). When newborn mice were injected intraperitoneally with MOL4070A retrovirus, almost all *SAMD9L*$^{+/-}$ (12 of 14) and *SAMD9L*$^{-/-}$ (10 of 12) mice died of nonlymphoid hematopoietic neoplasms (Figure 2A; Table S2), much earlier than mice that developed spontaneous myeloid malignancies (Figure 1F). In contrast, MOL4070A-infected *SAMD9L*$^{+/+}$ mice developed myeloid diseases at a significantly lower frequency (5 of 30; $p < 0.01$) within the 15-month observation period (Figure 2A).

Unlike uninfected *SAMD9L*-deficient mice, which preferentially developed MDS (13 of 30), 16 of 26 virus-infected mice showed myeloid leukemias of various types such as immature myeloid leukemia expressing myeloid (Gr1) and megakaryocyte (CD61) markers (Figure 2B, M-4), myelomonocytic leukemia with weak CD61 expression (M-20), and monocytic leukemia partially positive for B cell (B220), erythroid (Ter119), or megakaryocyte markers (M-26). Although leukemic cells from two *SAMD9L*$^{+/-}$ mice showed no SAMD9L protein (Figure 2C, M-15 and M-17) in immunoblots, long-distance PCR readily

amplified full-length *SAMD9L* DNA and mRNA that contained no mutation.

By the inverse PCR method (Yamashita et al., 2005), two common integration sites (CISs) were identified in leukemic samples from *SAMD9L*-deficient mice (Table S3), whereas no CIS was identified in samples from *SAMD9L*$^{+/+}$ mice. In six samples (M-9, M-17, M-19, M-20, M-24, and M-26), virus was found integrated into the *Evi1* gene (Figure 2D, upper) encoding a Zn finger transcription factor, whereas three additional samples (14%; M-4, M-18, and M-23) showed integration in the *Fbxl10* (also *JHDM1B*/*Ndy1*/*KDM2B*) gene (Frescas et al., 2007; Sánchez et al., 2007) (Figure 2D, lower), which encodes a histone H3K36 demethylase. Southern blot analysis showed polymorphic bands in all tumors (Figure 2E), indicating that the tumors were composed largely of cells with these integration sites. Quantitative real-time PCR analysis showed higher expression levels than the median level of *Evi1* mRNA in nonintegrated samples (Figure 2F, left), whereas two (M-4 and M-18) maintained higher *Fbxl10* mRNA levels relative to nonintegrated samples (Figure 2F, right panel).

Although Evi1 is well known to be overexpressed by retrovirus insertion in mouse myeloid leukemia, the frequency of 6 (27.2%) out of 22 myeloid malignancies carrying SAMD9L deficiency was remarkably high compared with other leukemogenic factors (usually around 5% or less) such as CBFβ-MYH11 (Castilla et al., 2004) and NUP98-HOXD13 (Slape et al., 2007). Enhancement of leukemia incidence in *SAMD9L*-deficient mice combined with *Evi1* or *Fbxl10* overexpression was further analyzed by retrovirus-mediated in vitro gene transfer experiments (see Experimental Procedures). Although no mice with transferred control *SAMD9L*$^{+/+}$GFP or *SAMD9L*$^{-/-}$GFP BM cells (BMCs) developed myeloid disorders during the 10-month observation period (Figure 2G), 3 of 11 mice with transferred *SAMD9L*$^{+/+}$*Evi1* cells died of hematopoietic malignancies (Table S4). This relatively low frequency of myeloid diseases induced by *Evi1* gene transfer is in agreement with previously published results by Buonamici et al. (2004), Cuenco and Ren (2004), and Watanabe-Okochi et al. (2008). In contrast, all mice (11 of 11) receiving transferred *SAMD9L*$^{-/-}$*Evi1* cells died of hematopoietic malignancies, particularly myeloid disorders (10 of 11; $p < 0.01$; Figure 2G, left). Although not a statistically significant result ($p = 0.082$), we also found that no mouse with transferred *SAMD9L*$^{+/+}$*Fbxl10* cells ($n = 12$) developed a hematopoietic malignancy, whereas 3 of 13 mice with transferred *SAMD9L*$^{-/-}$*Fbxl10* cells developed myeloid malignancies (Figure 2G, right panel).

SAMD9L Deficiency Affects Hematopoietic Stem Cells and Progenitors

Mouse (12 weeks old) BMCs were separated into three fractions: long term (LT)-LSK (CD34$^-$, CD135(Flt3)$^-$, lineage-negative [Lin$^-$], Sca-1$^+$, c-Kit$^+$); short term (ST)-LSK (CD34$^+$, CD135$^-$, LSK); and multipotent progenitor (MPP; CD34$^+$, CD135$^+$ LSK). Quantitative real-time PCR revealed that SAMD9L mRNA levels in *SAMD9L*$^{+/-}$ or *SAMD9L*$^{-/-}$ progenitors were roughly 50% or 0% of that in *SAMD9L*$^{+/+}$ cells, respectively (Figure 3A). Reduction of SAMD9L mRNA was supported by transcriptome analysis of LSK cells using a next-generation sequencer (Figure 3B), which also demonstrated that *SAMD9L* deficiency affects the expression of only a few genes (Table S5). In addition, the total number and proportion of the three LSK fractions in BM from *SAMD9L*-deficient mice were similar to those in BM from *SAMD9L*$^{+/+}$ mice (Figure 3C).

Despite these apparently small effects on the expression profile and the repertoire of early hematopoietic progenitors, colony-replating assay revealed prominent effects of *SAMD9L* deficiency. BMCs (12 weeks old) were grown in semisolid culture with appropriate cytokines, and colonies were counted and harvested for replating after 2 weeks. Although cells from *SAMD9L*$^{+/+}$ mice formed fewer colonies by the third replating (Figure 3D), cells from *SAMD9L*-deficient mice continued to form similar numbers and sizes of well-differentiated colonies beyond the seventh plating. The excess number of colonies formed was reduced by retrovirus-mediated forced expression of Samd9L (Figure 3E). These data suggested enhanced self-renewal and/or delays in differentiation of *SAMD9L*-deficient stem cells.

Enhanced reconstitution ability of stem cells was demonstrated by competitive repopulation assay using the Ly5 congenic mouse system. Irradiated Ly5.1 mice were transplanted with LT-LSK cells from *SAMD9L*$^{+/+}$ or *SAMD9L*-deficient Ly5.2 mice (10 weeks old) together with BMCs from *SAMD9L*$^{+/+}$Ly5.1 mice. Increased WBC numbers of *SAMD9L*-deficient cells relative to *SAMD9L*$^{+/+}$ cells were observed in recipient mice (Figure 3F). This was confirmed by limiting-dilution transplants using three dose concentrations of BMCs, results of which showed a higher frequency of multilineage repopulating cells (myeloid and T/B lymphocytes) at 8 weeks in *SAMD9L*$^{-/-}$ donor BM (Figure S1), suggesting enhanced reconstitution ability of stem cells and/or early hematopoietic progenitors.

In addition, growth advantage in the presence of cytokines was evident in liquid cultures of c-Kit$^+$ Lin$^-$ (KL) cells (Figure 3G), which were amplified by primary cultures of mouse BMCs using stem cell factor (SCF) and thrombopoietin (Kuribara et al., 2004). In this system, the level of SAMD9L expression in *SAMD9L*$^{+/-}$ KL cells was approximately 15% of that in *SAMD9L*$^{+/+}$ cells (Figure 3H).

Hypersensitivity of *SAMD9L*-deficient progenitors to cytokines was also shown in in vivo experiments (Figure 3I). Mice were injected with cyclophosphamide (CPA) (day 0) and human granulocyte colony-stimulating factor (hG-CSF) (days 1–4). WBC counts of control *SAMD9L*$^{+/+}$ mice without hG-CSF injection decreased rapidly until day 2 or 3 and then the counts gradually increased, whereas daily hG-CSF injection accelerated the recovery, as previously demonstrated by others (Hattori et al., 1990). *SAMD9L*-deficient mice showed significantly higher WBC counts at the nadir (day 3).

Because mice developed MDS at an old age, we examined the features of BM progenitors of old mice (26 months) by colony-replating assay. Cells from *SAMD9L*$^{+/+}$ non-MDS mice formed fewer primary colonies (Figure 3J), up to one-third of those from young mice (Figure 3D) probably due to aging, and colony formation potential was lost within replating five times. *SAMD9L*$^{+/-}$ non-MDS cells also formed fewer primary colonies; however, like *SAMD9L*-deficient cells from young mice, the colony formation potential was maintained during replating more than five times. Interestingly, cells from *SAMD9L*$^{+/-}$ MDS mice formed a reduced number of nonconcentric spread colonies, which were apparently different from colonies formed by non-MDS cells in shape (Figure 3K). These data suggested that additional abnormalities transform BM progenitors to MDS cells.

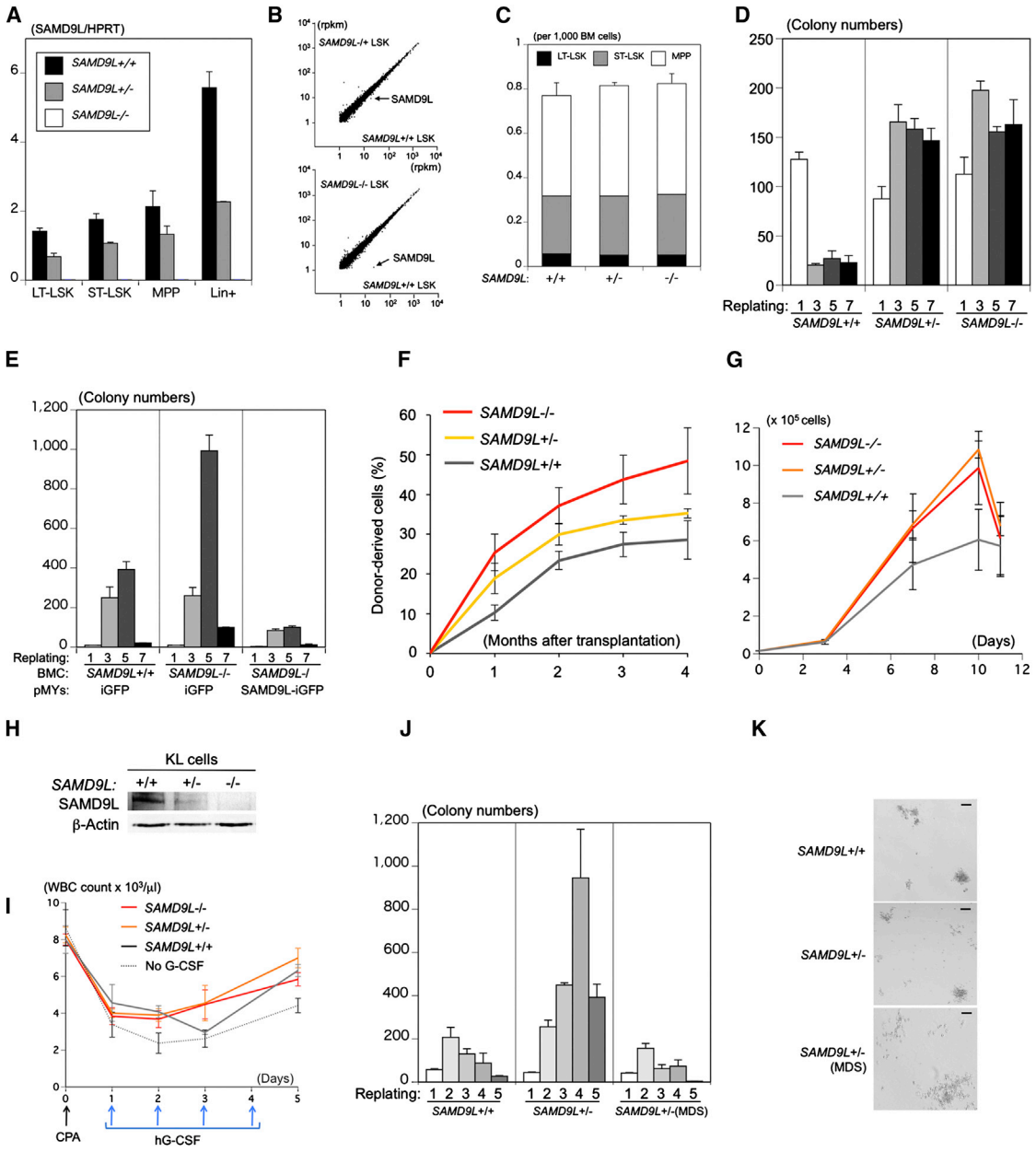

Figure 3. Hypersensitivity to Cytokines of SAMD9L-Deficient Hematopoietic Progenitors

(A) SAMD9 mRNA expression levels in hematopoietic cells are indicated below as a ratio relative to HPRT mRNA measured using quantitative real-time PCR. The mean and SD in four independent experiments are shown. Error bars, SD.

(B) Comprehensive identification and characterization of the transcriptome of LSK cells from *SAMD9L*-deficient BM are presented. Scatterplots of log10(rpkm) obtained for every transcript (>1 rpkm) in SAMD9L-deficient versus SAMD9L$^{+/+}$ LSK cells are shown.

(C) The numbers of each fraction of LSK cells per 1,000 BMCs are presented. A representative result is shown. Similar results were obtained in three independent experiments. Error bars, SD.

(D) The 2 × 10^4 BMCs obtained from 8-week-old *SAMD9L*$^{+/+}$, *SAMD9L*$^{+/-}$, and *SAMD9L*$^{-/-}$ mice were cultured in MethoCult M3434. Colonies were counted and replated at 2 × 10^4 cells every 2 weeks. Error bars, SD.

(E) BMCs were infected with pMYs retrovirus indicated below, and 0.7 × 10^4 c-Kit$^+$, GFP$^+$ cells were sorted and cultured in MethoCult M3434. Colonies were counted and replated at 2 × 10^4 cells every 10 days. iGFP, ires-GFP. Error bars, SD.

(F) Repopulation ability of *SAMD9L*$^{+/+}$, *SAMD9L*$^{+/-}$, and *SAMD9L*$^{-/-}$ LT-LSK cells isolated from 10-week-old mice is illustrated. The percentages of donor-derived (Ly5.2+) *SAMD9L*$^{+/-}$ and *SAMD9L*$^{-/-}$ cells in the total WBCs in the peripheral blood at periods indicated after transplantation are shown. Data are plotted as means with error bars (SD). Representative results from three independent experiments are shown.

(G) BMCs were harvested and cultured in the presence of SCF and thrombopoietin (TPO) for 5 days. KL cells were then selected and cultured in SCF- and TPO-containing medium. Cell numbers at the indicated period are shown. Error bars, SD.

(H) Immunoblot analysis of extracts from KL cells used SAMD9L (top) or β-actin (bottom) antibody. *SAMD9L* genotypes are indicated above.

(legend continued on next page)

To obtain candidates for such genomic abnormalities, we performed whole-exome sequencing on splenic cells from 17 mice that developed MDS or AML. We identified a total of 89 missense/nonsense/frameshift mutations that partially overlapped with genes (or closely related genes) mutated in human hematopoietic malignancies (Table S6).

SAMD9L Facilitates Homotypic Fusion of Endosomes

The above findings suggested that *SAMD9L* deficiency sensitizes hematopoietic progenitors to cytokines. KL cells (purity >90%) were harvested and starved of cytokines for 8 hr and then cultured in SCF-containing medium. In *SAMD9L*$^{+/+}$ KL cells, ERK was phosphorylated within 5 min of SCF stimulation (Figure 4A), followed by a rapid decline in phosphorylated-ERK (pERK) level. In contrast, KL cells obtained from *SAMD9L*-deficient mice maintained high levels of pERK even at 50 min after the addition of SCF. These data suggested that SAMD9L is involved in the turnover of cytokine receptors or negative feedback regulation for cytokine-derived signals.

A recent report demonstrated that hSAMD9L binds to an endosome protein, Rgl2 (Hershkovitz et al., 2011), which regulates cytokine receptor-derived signals (Takaya et al., 2007). Indeed, immunostaining using SAMD9L antibody showed a vesicular pattern of SAMD9L localization in approximately 15% of KL cells (Figure 4B, panel 1) or lung fibroblasts (panel 4) that overlapped with the localization of Rab5, an early endosomal protein (Bucci et al., 1992).

Ligand-bound cytokine/growth factor receptors are endocytosed and transitioned to endosomes and then degraded in lysosomes (Haas et al., 2005; Karlsson et al., 2006; Luzio et al., 2009). To analyze this process, we used lung fibroblasts expressing endogenous platelet-derived growth factor receptor (PDGFRβ) because sufficient numbers of cells can be obtained for pulse-chase experiments, and these cells have a large cytoplasmic volume allowing detailed observation of endosomes.

In pulse-chase studies, cell surface receptors were labeled with biotin, enabling us to discriminate cell surface and endocytosed receptors (Karlsson et al., 2006; Roberts et al., 2001) (see Experimental Procedures). Cell surface PDGFRβ was internalized within 5 min after PDGF stimulation of SAMD9$^{+/+}$ fibroblasts (Figure 4C, lanes 1–4), followed by an increase in endocytosed receptor levels after 15 min (lane 3), which then returned to low levels within 30 min (lane 4).

When we repeated this experiment using lung fibroblasts with reduced expression of SAMD9L by small hairpin RNA (sh#4 fibroblasts) (Figure 4D, lane 2), surface receptor levels in sh#4 fibroblasts behaved in a similar manner (Figure 4C, upper panel, lanes 5–8); however, these cells showed a 5-fold higher accumulation of endocytosed receptors relative to WT fibroblasts (lower panel, lanes 7 and 8). We established cells that coexpressed a FLAG-tagged sh#4-resistant SAMD9L (Figure 4D, lane 3) and found that endocytosed PDGFRβ accumulation was reduced to levels found in SAMD9L$^{+/+}$ fibroblasts (Figure 4C, lower panel, lanes 11 and 12), excluding the possibility of off-target effects.

We established lung fibroblasts from *SAMD9L*$^{+/-}$ and *SAMD9L*$^{-/-}$ mice, which expressed SAMD9L protein at levels of approximately 25% or 0%, respectively, of that in *SAMD9L*$^{+/+}$ mice (Figure 4E, top panel). Both *SAMD9L*$^{+/-}$ and *SAMD9L*$^{-/-}$ cells showed endocytosed receptor accumulation (Figure 4E, middle) and persistent phosphorylation of Akt (Figure 4E, bottom two panels) like sh#4 fibroblasts.

To elucidate the roles of SAMD9L in the metabolism of endocytosed PDGFRβ, we observed endosomes and lysosomes in lung fibroblasts expressing a myc-tagged PDGFRβ. In PDGF-starved fibroblasts, myc-PDGFRβ localized to the cell surface as well as to the cytoplasm with a diffuse and vesicular pattern (Figure 4F, panel 1), whereas an early endosome marker EEA1 localized to the cytoplasm (panel 5). PDGF stimulation for 5 min induced little change (Figure 4F, panels 2 and 6). However, upon PDGF treatment for 15 min, myc-PDGFRβ on the cell surface was barely visible, and relatively large vesicles (>1 μm) containing myc-PDGFRβ or EEA1 were observed in the perinuclear region (Figure 4F, panels 3, 3′, 7, and 7′; Figure 4G). Some regions (approximately 30%) within the large vesicles were positive for both EEA1 and PDGFR on immunostaining analyses (Figure 4F, panel 11′). Thirty minutes after the addition of PDGF, vesicle size decreased (Figure 4F, panels 4 and 8), and only a few vesicles were positive for both EEA1 and PDGFRβ (Figure 4F, panel 12). Instead of EEA1, lysosome-associated membrane protein 1 (Lamp1)-positive vesicles were fused to approximately 30% of those containing PDGFRβ (Figure 4H, panel 3). This time course is in agreement with a previous report by Karlsson et al. (2006), showing that early endosomes containing growth factor receptors increase in size via homotypic fusion and then transition to late endosomes that fuse with lysosomes.

We repeated this experiment using sh#4 fibroblasts. Although little difference was observed by PDGF stimulation for 5 min (Figure 4F, panel 14), after 15 min of PDGF treatment, PDGFRβ-containing vesicles moved to the perinuclear region, but these vesicles were noticeably smaller (Figure 4F, panels 15 and 15′; Figure 4G). Shrunken myc-PDGFR-containing vesicles in the perinuclear region were also observed in *SAMD9L*$^{+/-}$ and *SAMD9L*$^{-/-}$ fibroblasts 15 min after PDGF stimulation (Figure 4G). Thirty minutes after the addition of PDGF, few endosomes in sh#4 fibroblasts were positive for both Lamp1 and PDGFRβ (Figure 4H, panel 6), suggesting that SAMD9L promotes the fusion of early endosomes that will transition to late endosomes and/or lysosomes.

It was reported that EEA1 promotes homotypic fusion of endosomes (Christoforidis et al., 1999; Mills et al., 1998), and EEA1 downregulation delays the degradation of epidermal growth factor receptor (Leonard et al., 2008). Indeed, when EEA1 expression was downregulated using EEA1-specific siRNAs (Figure 5A), accumulation of endocytosed PDGFRβ and persistent phosphorylation of Akt were also evident 15 or 30 min after stimulation

(I) Mice (four each) were injected with CPA on day 0 and hG-CSF daily from day 1 to day 4. Average WBC counts and SD are shown.
(J) The 2 × 10^4 BMCs obtained from 26-month-old *SAMD9L*$^{+/+}$ non-MDS, *SAMD9L*$^{+/-}$ non-MDS, and *SAMD9L*$^{+/-}$ MDS mice were cultured in MethoCult M3434. Colonies were counted and replated at 2 × 10^4 cells every 10 days. Error bars, SD.
(K) Representative images show colonies obtained from 26-month-old mice. Scale bars, 100 μm.
See also Tables S5 and S6 and Figure S1.

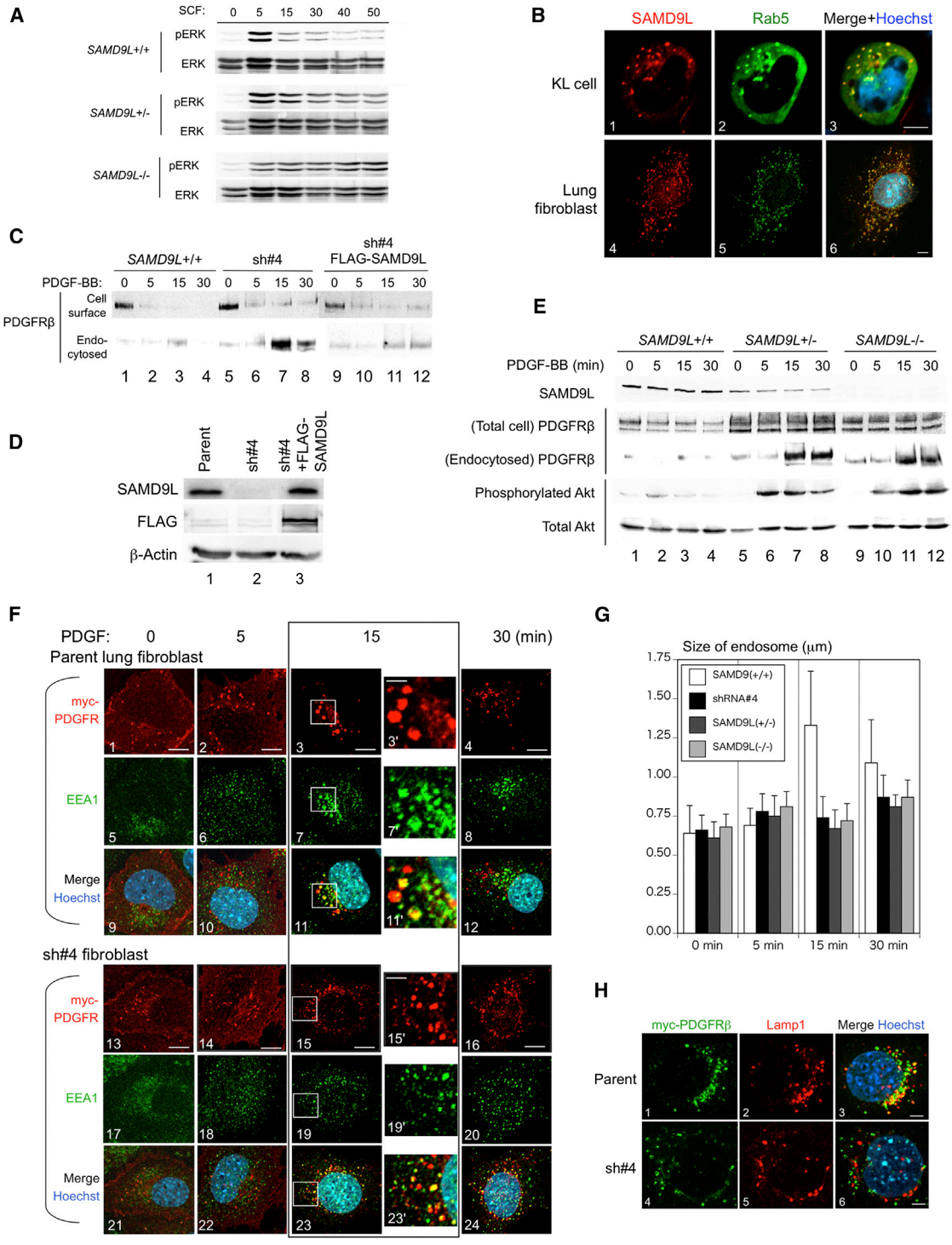

Figure 4. Involvement of SAMD9L in Homotypic Fusion of Endosomes

(A) KL cells from SAMD9L$^{+/+}$, SAMD9L$^{+/-}$, and SAMD9L$^{-/-}$ mice were SCF starved for 8 hr and then stimulated with SCF for the indicated number of minutes. The results of immunoblot detection of pERK and total ERK are shown.

(B) A KL cell (panels 1–3) or lung fibroblast (panels 4–6) was stained with SAMD9L and Rab5 antibodies. Scale bars, 5 μm.

(C) Immunoblot detection of cell surface and endosomal PDGFRβ that were biotinylated and precipitated separately is shown.

(D) Immunoblot analyses used SAMD9L (top), FLAG (middle), or β-actin (bottom) antibody to detect proteins in parent *SAMD9L*$^{+/+}$ lung fibroblasts (lane 1), cells in which SAMD9L expression was constitutively downregulated by sh#4 (lane 2), and cells simultaneously expressing sh#4 and FLAG-SAMD9L (sh#4 resistant) (lane 3).

(E) Immunoblot detection used the antibodies indicated on the left. Cell extracts from *SAMD9L*$^{+/+}$, *SAMD9L*$^{+/-}$, or *SAMD9L*$^{-/-}$ lung fibroblasts were subjected to immunoblot analysis except for the middle panel, in which biotinylated and precipitated endosomal PDGFRβ was used.

(legend continued on next page)

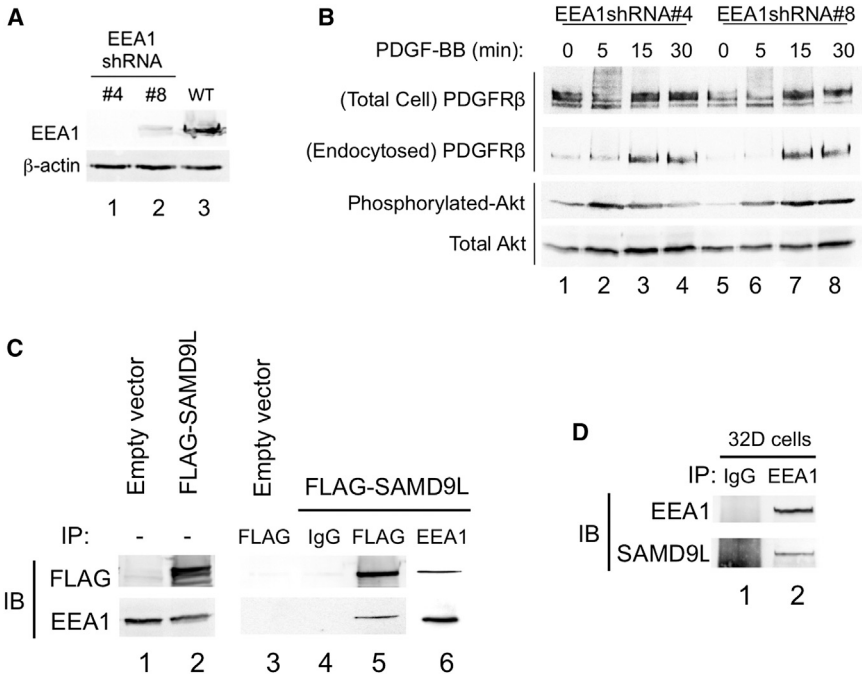

Figure 5. Involvement of SAMD9L in the Metabolism of Cytokine Receptor

(A) Immunoblot analyses used EEA1 (top) or β-actin (bottom) antibody to detect proteins in lung fibroblasts treated with EEA1 shRNA#4 (lane 1) or shRNA#8 (lane 2), and in parental cells (lane 3).

(B) Immunoblot detection used the antibodies indicated on the left. Cell extracts from lung fibroblasts expressing shRNA#4 (lanes 1–4) and shRNA#8 (lanes 5–8) were subjected to immunoblot analysis except for the middle panel, in which biotinylated and precipitated endosomal PDGFRβ was used.

(C) 293 cells were transiently transfected with either empty p3×FLAG-CMV10 or p3×FLAG-CMV10-SAMD9L vector. Whole-cell extracts (lanes 1 and 2) or immunoprecipitated products (IP) using control IgG, FLAG, or EEA1 antibody were subjected to immunoblot analysis (IB) using antibodies indicated on the left.

(D) IP of 32D cells using antibodies in (C) were subjected to IB using antibodies indicated on the left.

with PDGF (Figure 5B, upper- and lower-middle panels, lanes 3, 4, 7, and 8). By coimmunoprecipitation analyses, we obtained data showing that SAMD9L binds to EEA1 in 293 cells (Figure 5C, lanes 5 and 6) or 32D myeloid cells (Figure 5D), suggesting that SAMD9L and EEA1 are crucial components of a protein complex that facilitate the degradation of cytokine receptors through the homotypic fusion of endosomes.

Application of the Results in Mice to Human Myeloid Malignancies with –7/7q–

In human, the related *SAMD9* (*hSAMD9*) gene in addition to *SAMD9L* (*hSAMD9L*) was expressed in hematopoietic progenitors (Figure 6A). The unusual gene distribution among mammals (see Introduction) suggests that SAMD9 and SAMD9L at least partially complement each other's functions. We introduced FLAG-tagged *hSAMD9* or *hSAMD9L* transgenes into lung fibroblasts established from *SAMD9L*$^{-/-}$ mice (Figure 6B). Relative to *SAMD9L*$^{-/-}$ cells infected with empty virus (Figure 6C, lanes 7 and 8), those expressing hSAMD9 or hSAMD9L showed a 10- or 3-fold decrease in endosomal PDGFRβ (Figure 6C, lanes 11 and 12, and 15 and 16), respectively, suggesting that hSAMD9 or hSAMD9L also downregulates cytokine signalings. In addition, coimmunoprecipitation analyses revealed that both hSAMD9 and hSAMD9L interact with EEA1 (Figure 6D, lanes 4, 6, and 10).

To test whether SAMD9L plays roles in cytokine-emanating signal transduction in human leukemia cells harboring monosomy 7, F-36P cells (Chiba et al., 1991) were infected with virus containing SAMD9L cDNA (Figure 6E, left panel). In cells infected with empty virus, substantial levels of ERK phosphorylation continued to be observed more than 1 hr after GM-CSF stimulation (Figure 6E, middle panels). However, ERK phosphorylation decreased to less than 10% within 30 min in cells expressing SAMD9L (Figure 6E, right).

We determined the copy number of *SAMD9* and *SAMD9L* genes in 60 unselected MDS and AML samples using mCGH and qPCR (Asou et al., 2009). A total of 17 patients (17 of 60, 28%) carried one copy each of the *SAMD9* and *SAMD9L* genes. The remaining 43 patients had two or more copies of both *SAMD9* and *SAMD9L* genes, and no patient harbored missense or nonsense mutations. Quantitative real-time PCR revealed that *SAMD9* or *SAMD9L* mRNA expression levels in BM mononuclear cells in patients with MDS/AML with one gene copy were significantly reduced relative to those carrying two or more copies ($p < 0.01$; Figure 6F). Intriguingly, the mRNA expression level of *SAMD9* correlated with that of *SAMD9L* in MDS/AML cells (Figure 6G), suggesting that loss of one 7q allele results in simultaneous reductions in *SAMD9* and *SAMD9L* expression.

To test whether *Evi1* or *Fbxl10* overexpression contributes to human leukemogenesis associated with −7/7q−, as they did in *SAMD9L*-deficient mice (Figure 2F), we measured *Evi1* and *Fbxl10* mRNA levels in patients with MDS/AML. *Evi1* expression levels were higher (>0.5 of HPRT expression levels) in 5 of 17 (29%) and 3 of 43 (7.0%) samples carrying haploid or diploid/polyploid for *SAMD9*/*SAMD9L* genes, respectively

(F) Lung fibroblasts expressing myc-PDGFRβ (panels 1–12) and those expressing reduced levels of SAMD9L (sh#4; panels 13–24) were starved of PDGF for 16 hr, followed by stimulation with 100 ng/ml PDGF-BB for the indicated lengths of time. Cells were stained with the antibodies indicated on the left. Panels 3′, 7′, 11′, 15′, 19′, and 23′ show 5-fold enlargements of endosome-rich regions. Scale bars, 10 μm.

(G) Longitudinal diameter of PDGFR-positive endosomes was measured using ImageJ software (mean and SD of 200 endosomes).

(H) Cells stimulated with 100 ng/ml PDGF-BB for 30 min were stained with Myc and Lamp1 antibodies. Scale bars, 5 μm.

Nuclei were stained with Hoechst 33342 in (B), (F), and (H).

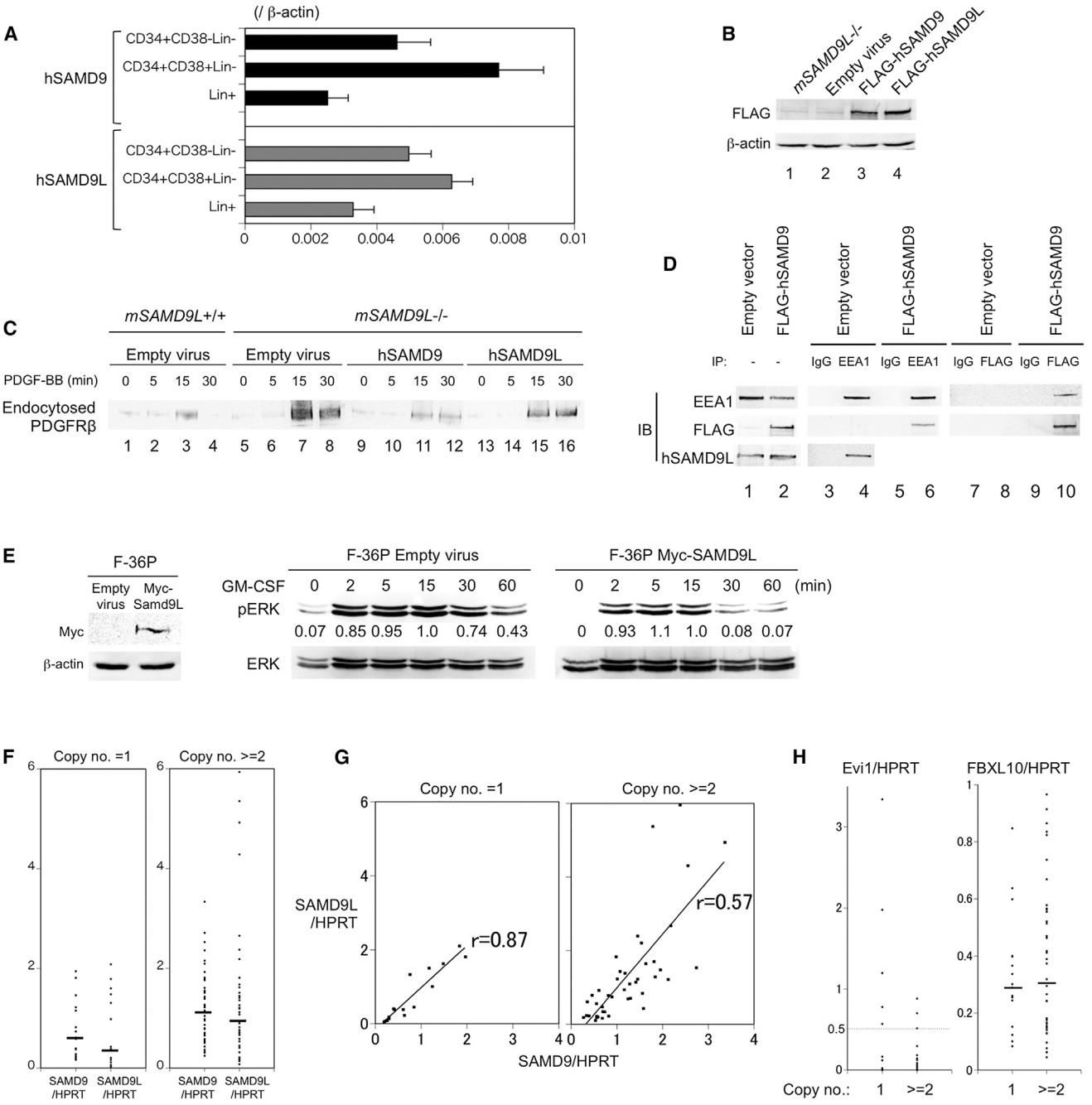

Figure 6. Function and Expression of hSAMD9 and hSAMD9L

(A) SAMD9 (top) and SAMD9L (bottom) mRNA expression levels in hematopoietic cells are indicated on the left as a ratio relative to β-actin mRNA measured using quantitative real-time PCR. The mean and SEM in four independent experiments are shown.

(B) Immunoblot analysis used FLAG (upper) or β-actin (bottom) antibody. Lung fibroblasts from *SAMD9L*$^{-/-}$ mice (lane 1), cells infected with the empty pMXs (lane 2), pMXs-FLAG-hSAMD9 (lane 3), or pMXs-FLAG-hSAMD9L (lane 4) virus are shown.

(C) Lung fibroblasts from SAMD9L$^{+/+}$ mice infected with the empty pMXs virus (lanes 1–4), fibroblasts from SAMD9L$^{-/-}$ mice infected with the empty pMXs (lanes 5–8), pMXs-FLAG-hSAMD9 (lanes 9–12), and pMXs-FLAG-hSAMD9L (lanes 13–16) virus are presented. Cells were starved of PDGF for 16 hr and then stimulated with PDGF-BB (100 ng/ml) for the periods indicated above. Immunoblot detection of endosomal PDGFRβ is shown.

(D) 293 cells were transiently transfected with either empty p3×FLAG-CMV10 or p3×FLAG-CMV10-SAMD9L vector. Whole-cell extracts (lanes 1 and 2) or immunoprecipitated products using control IgG, FLAG, or EEA1 antibody were subjected to immunoblot analysis using EEA1 (top), FLAG (middle), or hSAMD9L (bottom) antibody.

(E) F-36P cells were infected with empty retrovirus or virus containing mouse SAMD9L cDNA and cytokine starved for 12 hr and then stimulated with SCF for the indicated number of minutes. The results of immunoblot detection of pERK and total ERK (left and middle), and myc and β-actin (right) are shown.

(legend continued on next page)

($p < 0.05$, chi-square test; Figure 6H, left), consistent with previous reports by Barjesteh van Waalwijk van Doorn-Khosrovani et al. (2003) and Lugthart et al. (2008). In contrast, there was no significant difference in Fbxl10 mRNA expression levels (Figure 6H, right).

DISCUSSION

In this paper, we demonstrated that *SAMD9L* haploinsufficiency ultimately induces the development of myeloid diseases in mice. Because humans have the related *SAMD9* gene that encodes a protein that compensates for the function of SAMD9L at least in part, loss of one copy of each of the *SAMD9* and *SAMD9L* genes (i.e., *SAMD9*$^{+/-}$*SAMD9L*$^{+/-}$) as a result of −7/7q− may not correspond to *SAMD9L*$^{+/-}$ in mice. However, simultaneous reduction of SAMD9 and SAMD9L mRNA by loss of 7q (Figure 6F) suggests that SAMD9/SAMD9L function in human cells harboring −7/7q− is parallel to SAMD9L function in *SAMD9L*$^{+/-}$ mouse cells.

SAMD9L haploinsufficiency in the natural course induced the development of MDS in elderly mice (Figure 1F), mimicking the typical clinical association between monosomy 7 as a sole anomaly and sporadic MDS in elderly humans (Jaffe et al., 2001). Enhancement of stem cell self-renewal and/or delay in differentiation of early progenitors was observed in both young and old SAMD9L$^{+/-}$ non-MDS mice (Figures 3D and 3J); however, BMCs from old SAMD9L$^{+/-}$ MDS mice lost these features. This suggests that additional genetic and/or epigenetic alterations (other than age-related ones) that suppress stem cell self-renewal and/or induce differentiation of early progenitors play critical roles in the development of MDS. We consider that *SAMD9L* haploinsufficiency contributes to MDS by protecting stem cell(s) harboring such MDS-causative genetic and/or epigenetic alterations from depletion.

In addition to sporadic MDS in elderly individuals, −7/7q− frequently occurs in younger patients during the advancement of secondary AML/MDS in radiation-induced and therapy-related cases (Pedersen-Bjergaard et al., 2008), as well as during the development of AML/MDS among patients with a propensity for myeloid diseases such as patients with Fanconi anemia and congenital neutropenia. −7/7q− is also often detected as an additional chromosome abnormality in patients with AML harboring a variety of leukemogenic chromosome translocations and well-known gene abnormalities including Evi1 overexpression (Barjesteh van Waalwijk van Doorn-Khosrovani et al., 2003; Jaffe et al., 2001; Lugthart et al., 2008). The role of −7/7q− that promotes leukemogenesis caused by such a wide variety of genetic alterations to different subtypes of myeloid malignancies appears to correspond to the potential of *SAMD9L* haploinsufficiency that promotes diverse pathways activated by retrovirus insertion toward different types of myeloid leukemia in younger mice (Figures 2A and 2B; Table S2).

SAMD9L haploinsufficiency sensitized hematopoietic progenitors to cytokines both in vitro and in vivo (Figures 3G and 3I). This is consistent with a previous report indicating that G-CSF preferentially stimulates proliferation of monosomy 7 progenitors carrying nonmutated G-CSF receptor (Sloand et al., 2006). In addition, a correlation has been reported between the development of myeloid malignancies harboring monosomy 7 and LT treatment of aplastic anemia and congenital neutropenia with G-CSF (Kojima et al., 2002; Weinblatt et al., 1995), supporting that the loss of *SAMD9/SAMD9L* genes plays crucial roles in the growth advantage under the presence of cytokines and leukemogenic process of progenitors harboring −7/7q−.

The presence of broad and divergent deletion regions in patients with 7q− AML/MDS suggests that the total loss of one tumor suppressor gene (which usually occurs by the deletion of one allele and a mutation in the other) is unlikely to be responsible for myeloid transformation by −7/7q− (Jerez et al., 2012). Rather, like current models proposed for 5q− (another large deletion frequently found in MDS; Brunning et al., 2008), haploinsufficiencies of multiple genes play critical roles in the promotion of myeloid diseases (Ebert, 2009). The 5q− region encodes multiple (candidate) causative proteins that carry out a broad spectrum of biochemical functions. Haploinsufficiency of each gene is likely responsible for the corresponding clinical symptoms, such as anemia, thrombocytosis, clonal dominance, and response to lenalidomide (a key drug for treating 5q− MDS).

We consider that *SAMD9/SAMD9L* and *Miki*, the latter of which we recently reported as being involved in the abnormal morphology characteristic of MDS (Ozaki et al., 2012), are members of multiple causative genes on 7q, whose haploinsufficiency in combination plays crucial roles in the development of myeloid malignancies. Because SAMD9 and SAMD9L compensate each other's function at least in part, heterozygous loss of both *SAMD9* and *SAMD9L* genes may be required to develop human myeloid diseases, and that is why mutations have not been identified in either gene. Careful analysis of small deletions and mutations using high-throughput sequencing may help to identify other key genes in this region that contribute to myeloid transformation by loss of one 7q allele.

EXPERIMENTAL PROCEDURES

Mouse Experiments

SAMD9L-deficient mice were established according to standard procedures described in Supplemental Experimental Procedures. *Evi1* gene transduction was performed according to the method described previously by Jin et al. (2007). *Fbxl10* transduction was performed using the method described in Supplemental Experimental Procedures. Newborn mice were inoculated intraperitoneally with 100 μl MOL4070A retrovirus solution containing approximately 1×10^5 infectious particles. Retroviral integration sites were identified using iPCR as described previously by Yamashita et al. (2005). Peripheral blood chimerisms of the recipient mice were analyzed as previously described (Nagamachi et al., 2010). To analyze the effect of hG-CSF, mice (9 weeks of age) that had been intraperitoneally injected with CPA (Shionogi Pharmaceuticals, Osaka) at a dose of 100 mg/kg on day 0, were given 0.1 μg of human G-CSF (Miltenyi Biotec, Bergisch Gladbach) per mouse per day, or control vehicle for 4 days from day 1 to day 4. Blood samples for the measurement

(F) Ratios of *SAMD9* and *SAMD9L* mRNAs relative to HPRT mRNA in the BM-MNC of patients with MDS/AML that are *SAMD9/SAMD9L* haploid (left) or diploid/polyploid (right) are shown. Horizontal lines indicate the median.
(G) Correlation between the relative expression levels of *SAMD9* (horizontal) and *SAMD9L* (vertical) mRNA to HPRT mRNA from MNCs described in (F) is presented. Regression lines and correlation coefficient (r) are indicated.
(H) Relative expression levels of Evi1 (left) and Fbxl10 (right) mRNA to HPRT mRNA in MNCs of patients with MDS/AML described in (F) are shown.

of WBC count were obtained 5 hr after each injection and 30 hr after the injection on day 4. All mice were kept according to guidelines of the Institute of Laboratory Animal Science, Hiroshima University. The Animal Care Committee at the Japanese Foundation for Cancer Research approved all murine studies.

Cells and Cell Culture

F-36P cells were cultured in medium described by others (Chiba et al., 1991). Lung fibroblasts and 293 cells and their derivatives were grown in DMEM supplemented with 10% FBS. LSK cells were isolated and characterized (Honda et al., 2011; Mizuno et al., 2008), using antibodies listed in Supplemental Experimental Procedures. Human $CD34^+$ $CD38^-$ Lin^-, $CD34^+$ $CD38^+$ Lin^-, and Lin^+ cells were isolated from cryopreserved human BM cells (TaKaRa Bio, Shiga) (Shima et al., 2010). The stained cells were analyzed and sorted by FACSAria II (BD Biosciences). c-Kit^+ BM cells expressing Samd9L were obtained by infecting cells with pMYs retrovirus carrying *SAMD9L* cDNA and *IRES-GFP* followed by sorting with GFP. Cells stably expressing PDGFRβ and SAMD9/SAMD9L proteins were established by infecting cells with pMXs retrovirus carrying the corresponding cDNA followed by selection with neomycin. Cells expressing mouse SAMD9L or EEA1 at reduced levels were generated using U3-deleted pMX-puro retrovirus carrying a mouse U6 promoter and a small hairpin sequence specific for mouse SAMD9L mRNA (sh#4, target sequence: ACAATGGAGTGATCTACTACA), or EEA1 mRNA (sh#4, CAAGAAAGCATAAA GGAAATA; sh#8, CGGAGAAGCTGAAGAATCAGT). sh#4-resistant mouse *SAMD9L* cDNA was created by replacing nucleotides in the target sequence to CAgTGGAGcGAcCTtCTt (underline indicates replaced nucleotides), changes that do not affect the amino acid sequence. Murine colony formation assays were performed using MethoCult M3434 (STEMCELL Technologies, Vancouver) according to the manufacturer's instructions.

Quantitative Real-Time PCR, Transcriptome Analysis, Whole-Exome Sequencing, and Determination of Copy Number

Total RNA was extracted from sorted LSK cells using RNeasy Micro Kit (QIAGEN, Tokyo), and mRNA was purified using SuperScript VILO (Invitrogen, Venlo). Quantitative real-time PCR was performed as previously described by Kuribara et al. (2004) using the primer sets listed in a table in Supplemental Experimental Procedures. Transcriptome analysis was performed using a next-generation sequencer (GAIIx; Illumina, San Diego) according to the manufacturer's instructions. The generated sequence tags were mapped onto the mouse genomic sequence (UCSC Genome Browser, version mm9) using the sequence alignment program ELAND (Illumina). Whole-exome sequencing was performed according to the method described in Supplemental Experimental Procedures. Copy numbers of *hSAMD9* and *hSAMD9L* genes were determined using mCGH and qPCR techniques as previously described (Asou et al., 2009).

Protein Analysis

Immunoprecipitation and immunoblot analyses and immunostaining were performed according to standard procedures by Mizuno et al. (2008) and Shinjyo et al. (2001). Cell surface and internalized PDGFRβ were isolated as previously published procedures by others (Karlsson et al., 2006; Roberts et al., 2001) and are described in Supplemental Experimental Procedures.

Human Samples

Written informed consent was obtained from patients with AML/MDS in accordance with the Declaration of Helsinki for BM sampling, and analysis was undertaken with the approval of the Hiroshima University institutional review board.

ACCESSION NUMBERS

The short-read sequence archive data appearing in this paper were registered in GenBank/DDBJ under the following accession numbers: DRA000636, DRA000637, and DRA000638.

SUPPLEMENTAL INFORMATION

Supplemental Information includes Supplemental Experimental Procedures, one figure, and six tables and can be found with this article online at http://dx.doi.org/10.1016/j.ccr.2013.08.011.

ACKNOWLEDGMENTS

We would like to thank Drs. M. Iwama for providing virus and methods for gene transfer to mouse bone marrow cells and Y. Ebihara for useful discussion. We thank Mrs. M. Nakamura, Mr. N. Yamasaki, and Mrs. R. Tai for excellent technical assistance. This work was supported by Grants-in-Aid for Scientific Research from the Ministry of Education, Culture, Sports, Science and Technology of Japan.

Received: July 13, 2011
Revised: December 25, 2012
Accepted: August 15, 2013
Published: September 9, 2013

REFERENCES

Asou, H., Matsui, H., Ozaki, Y., Nagamachi, A., Nakamura, M., Aki, D., and Inaba, T. (2009). Identification of a common microdeletion cluster in 7q21.3 subband among patients with myeloid leukemia and myelodysplastic syndrome. Biochem. Biophys. Res. Commun. *383*, 245–251.

Barjesteh van Waalwijk van Doorn-Khosrovani, S., Erpelinck, C., van Putten, W.L., Valk, P.J., van der Poel-van de Luytgaarde, S., Hack, R., Slater, R., Smit, E.M., Beverloo, H.B., Verhoef, G., et al. (2003). High EVI1 expression predicts poor survival in acute myeloid leukemia: a study of 319 de novo AML patients. Blood *101*, 837–845.

Brunning, R., Germing, U., Le Beau, M.M., Porwit, A., Baumann, I., Vardiman, J.W., and Hellstrom-Lindberg, E. (2008). Myelodysplastic syndromes/neoplasms, overview. In WHO Classification of Tumours of Haematopoietic and Lymphoid Tissues, Fourth Edition, S.H. Swerdlow, International Agency for Research on Cancer., and World Health Organization., eds. (Lyon: IARC Press), pp. 62–73.

Bucci, C., Parton, R.G., Mather, I.H., Stunnenberg, H., Simons, K., Hoflack, B., and Zerial, M. (1992). The small GTPase rab5 functions as a regulatory factor in the early endocytic pathway. Cell *70*, 715–728.

Buonamici, S., Li, D., Chi, Y., Zhao, R., Wang, X., Brace, L., Ni, H., Saunthararajah, Y., and Nucifora, G. (2004). EVI1 induces myelodysplastic syndrome in mice. J. Clin. Invest. *114*, 713–719.

Castilla, L.H., Perrat, P., Martinez, N.J., Landrette, S.F., Keys, R., Oikemus, S., Flanegan, J., Heilman, S., Garrett, L., Dutra, A., et al. (2004). Identification of genes that synergize with Cbfb-MYH11 in the pathogenesis of acute myeloid leukemia. Proc. Natl. Acad. Sci. USA *101*, 4924–4929.

Chefetz, I., Ben Amitai, D., Browning, S., Skorecki, K., Adir, N., Thomas, M.G., Kogleck, L., Topaz, O., Indelman, M., Uitto, J., et al. (2008). Normophosphatemic familial tumoral calcinosis is caused by deleterious mutations in SAMD9, encoding a TNF-alpha responsive protein. J. Invest. Dermatol. *128*, 1423–1429.

Chiba, S., Takaku, F., Tange, T., Shibuya, K., Misawa, C., Sasaki, K., Miyagawa, K., Yazaki, Y., and Hirai, H. (1991). Establishment and erythroid differentiation of a cytokine-dependent human leukemic cell line F-36: a parental line requiring granulocyte-macrophage colony-stimulating factor or interleukin-3, and a subline requiring erythropoietin. Blood *78*, 2261–2268.

Christoforidis, S., McBride, H.M., Burgoyne, R.D., and Zerial, M. (1999). The Rab5 effector EEA1 is a core component of endosome docking. Nature *397*, 621–625.

Cuenco, G.M., and Ren, R. (2004). Both AML1 and EVI1 oncogenic components are required for the cooperation of AML1/MDS1/EVI1 with BCR/ABL in the induction of acute myelogenous leukemia in mice. Oncogene *23*, 569–579.

Ebert, B.L. (2009). Deletion 5q in myelodysplastic syndrome: a paradigm for the study of hemizygous deletions in cancer. Leukemia *23*, 1252–1256.

Frescas, D., Guardavaccaro, D., Bassermann, F., Koyama-Nasu, R., and Pagano, M. (2007). JHDM1B/FBXL10 is a nucleolar protein that represses transcription of ribosomal RNA genes. Nature *450*, 309–313.

Haas, A.K., Fuchs, E., Kopajtich, R., and Barr, F.A. (2005). A GTPase-activating protein controls Rab5 function in endocytic trafficking. Nat. Cell Biol. *7*, 887–893.

Hattori, K., Shimizu, K., Takahashi, M., Tamura, M., Oheda, M., Ohsawa, N., and Ono, M. (1990). Quantitative in vivo assay of human granulocyte colony-stimulating factor using cyclophosphamide-induced neutropenic mice. Blood *75*, 1228–1233.

Hershkovitz, D., Gross, Y., Nahum, S., Yehezkel, S., Sarig, O., Uitto, J., and Sprecher, E. (2011). Functional characterization of SAMD9, a protein deficient in normophosphatemic familial tumoral calcinosis. J. Invest. Dermatol. *131*, 662–669.

Honda, H., Takubo, K., Oda, H., Kosaki, K., Tazaki, T., Yamasaki, N., Miyazaki, K., Moore, K.A., Honda, Z., Suda, T., and Lemischka, I.R. (2011). Hemp, an mbt domain-containing protein, plays essential roles in hematopoietic stem cell function and skeletal formation. Proc. Natl. Acad. Sci. USA *108*, 2468–2473.

Jaffe, E.S., Harris, N.L., Stein, H., and Vardiman, J.M. (2001). Pathology and Genetics of Tumours of Haematopoietic and Lymphoid Tissues (Lyon: IARC press).

Jerez, A., Sugimoto, Y., Makishima, H., Verma, A., Jankowska, A.M., Przychodzen, B., Visconte, V., Tiu, R.V., O'Keefe, C.L., Mohamedali, A.M., et al. (2012). Loss of heterozygosity in 7q myeloid disorders: clinical associations and genomic pathogenesis. Blood *119*, 6109–6117.

Jiang, Q., Quaynor, B., Sun, A., Li, Q., Matsui, H., Honda, H., Inaba, T., Sprecher, E., and Uitto, J. (2011). The Samd9L gene: transcriptional regulation and tissue-specific expression in mouse development. J. Invest. Dermatol. *131*, 1428–1434.

Jin, G., Yamazaki, Y., Takuwa, M., Takahara, T., Kaneko, K., Kuwata, T., Miyata, S., and Nakamura, T. (2007). Trib1 and Evi1 cooperate with Hoxa and Meis1 in myeloid leukemogenesis. Blood *109*, 3998–4005.

Johnson, E., and Cotter, F.E. (1997). Monosomy 7 and 7q—associated with myeloid malignancy. Blood Rev. *11*, 46–55.

Karlsson, S., Kowanetz, K., Sandin, A., Persson, C., Ostman, A., Heldin, C.H., and Hellberg, C. (2006). Loss of T-cell protein tyrosine phosphatase induces recycling of the platelet-derived growth factor (PDGF) beta-receptor but not the PDGF alpha-receptor. Mol. Biol. Cell *17*, 4846–4855.

Kogan, S.C., Ward, J.M., Anver, M.R., Berman, J.J., Brayton, C., Cardiff, R.D., Carter, J.S., de Coronado, S., Downing, J.R., Fredrickson, T.N., et al.; Hematopathology subcommittee of the Mouse Models of Human Cancers Consortium. (2002). Bethesda proposals for classification of nonlymphoid hematopoietic neoplasms in mice. Blood *100*, 238–245.

Kojima, S., Ohara, A., Tsuchida, M., Kudoh, T., Hanada, R., Okimoto, Y., Kaneko, T., Takano, T., Ikuta, K., and Tsukimoto, I.; Japan Childhood Aplastic Anemia Study Group. (2002). Risk factors for evolution of acquired aplastic anemia into myelodysplastic syndrome and acute myeloid leukemia after immunosuppressive therapy in children. Blood *100*, 786–790.

Kuribara, R., Honda, H., Matsui, H., Shinjyo, T., Inukai, T., Sugita, K., Nakazawa, S., Hirai, H., Ozawa, K., and Inaba, T. (2004). Roles of Bim in apoptosis of normal and Bcr-Abl-expressing hematopoietic progenitors. Mol. Cell. Biol. *24*, 6172–6183.

Leonard, D., Hayakawa, A., Lawe, D., Lambright, D., Bellve, K.D., Standley, C., Lifshitz, L.M., Fogarty, K.E., and Corvera, S. (2008). Sorting of EGF and transferrin at the plasma membrane and by cargo-specific signaling to EEA1-enriched endosomes. J. Cell Sci. *121*, 3445–3458.

Li, C.F., MacDonald, J.R., Wei, R.Y., Ray, J., Lau, K., Kandel, C., Koffman, R., Bell, S., Scherer, S.W., and Alman, B.A. (2007). Human sterile alpha motif domain 9, a novel gene identified as down-regulated in aggressive fibromatosis, is absent in the mouse. BMC Genomics *8*, 92.

Lugthart, S., van Drunen, E., van Norden, Y., van Hoven, A., Erpelinck, C.A., Valk, P.J., Beverloo, H.B., Löwenberg, B., and Delwel, R. (2008). High EVI1 levels predict adverse outcome in acute myeloid leukemia: prevalence of EVI1 overexpression and chromosome 3q26 abnormalities underestimated. Blood *111*, 4329–4337.

Luzio, J.P., Parkinson, M.D., Gray, S.R., and Bright, N.A. (2009). The delivery of endocytosed cargo to lysosomes. Biochem. Soc. Trans. *37*, 1019–1021.

Mills, I.G., Jones, A.T., and Clague, M.J. (1998). Involvement of the endosomal autoantigen EEA1 in homotypic fusion of early endosomes. Curr. Biol. *8*, 881–884.

Mizuno, T., Yamasaki, N., Miyazaki, K., Tazaki, T., Koller, R., Oda, H., Honda, Z.I., Ochi, M., Wolff, L., and Honda, H. (2008). Overexpression/enhanced kinase activity of BCR/ABL and altered expression of Notch1 induced acute leukemia in p210BCR/ABL transgenic mice. Oncogene *27*, 3465–3474.

Nagamachi, A., Htun, P.W., Ma, F., Miyazaki, K., Yamasaki, N., Kanno, M., Inaba, T., Honda, Z., Okuda, T., Oda, H., et al. (2010). A 5′ untranslated region containing the IRES element in the Runx1 gene is required for angiogenesis, hematopoiesis and leukemogenesis in a knock-in mouse model. Dev. Biol. *345*, 226–236.

Ozaki, Y., Matsui, H., Asou, H., Nagamachi, A., Aki, D., Honda, H., Yasunaga, S., Takihara, Y., Yamamoto, T., Izumi, S., et al. (2012). Poly-ADP ribosylation of Miki by tankyrase-1 promotes centrosome maturation. Mol. Cell *47*, 694–706.

Pedersen-Bjergaard, J., Andersen, M.K., Andersen, M.T., and Christiansen, D.H. (2008). Genetics of therapy-related myelodysplasia and acute myeloid leukemia. Leukemia *22*, 240–248.

Roberts, M., Barry, S., Woods, A., van der Sluijs, P., and Norman, J. (2001). PDGF-regulated rab4-dependent recycling of alphavbeta3 integrin from early endosomes is necessary for cell adhesion and spreading. Curr. Biol. *11*, 1392–1402.

Sánchez, C., Sánchez, I., Demmers, J.A., Rodriguez, P., Strouboulis, J., and Vidal, M. (2007). Proteomics analysis of Ring1B/Rnf2 interactors identifies a novel complex with the Fbxl10/Jhdm1B histone demethylase and the Bcl6 interacting corepressor. Mol. Cell. Proteomics *6*, 820–834.

Shima, H., Takubo, K., Tago, N., Iwasaki, H., Arai, F., Takahashi, T., and Suda, T. (2010). Acquisition of G_0 state by CD34-positive cord blood cells after bone marrow transplantation. Exp. Hematol. *38*, 1231–1240.

Shinjyo, T., Kuribara, R., Inukai, T., Hosoi, H., Kinoshita, T., Miyajima, A., Houghton, P.J., Look, A.T., Ozawa, K., and Inaba, T. (2001). Downregulation of Bim, a proapoptotic relative of Bcl-2, is a pivotal step in cytokine-initiated survival signaling in murine hematopoietic progenitors. Mol. Cell. Biol. *21*, 854–864.

Slape, C., Hartung, H., Lin, Y.W., Bies, J., Wolff, L., and Aplan, P.D. (2007). Retroviral insertional mutagenesis identifies genes that collaborate with NUP98-HOXD13 during leukemic transformation. Cancer Res. *67*, 5148–5155.

Sloand, E.M., Yong, A.S., Ramkissoon, S., Solomou, E., Bruno, T.C., Kim, S., Fuhrer, M., Kajigaya, S., Barrett, A.J., and Young, N.S. (2006). Granulocyte colony-stimulating factor preferentially stimulates proliferation of monosomy 7 cells bearing the isoform IV receptor. Proc. Natl. Acad. Sci. USA *103*, 14483–14488.

Takaya, A., Kamio, T., Masuda, M., Mochizuki, N., Sawa, H., Sato, M., Nagashima, K., Mizutani, A., Matsuno, A., Kiyokawa, E., and Matsuda, M. (2007). R-Ras regulates exocytosis by Rgl2/Rlf-mediated activation of RalA on endosomes. Mol. Biol. Cell *18*, 1850–1860.

Topaz, O., Indelman, M., Chefetz, I., Geiger, D., Metzker, A., Altschuler, Y., Choder, M., Bercovich, D., Uitto, J., Bergman, R., et al. (2006). A deleterious mutation in SAMD9 causes normophosphatemic familial tumoral calcinosis. Am. J. Hum. Genet. *79*, 759–764.

Watanabe-Okochi, N., Kitaura, J., Ono, R., Harada, H., Harada, Y., Komeno, Y., Nakajima, H., Nosaka, T., Inaba, T., and Kitamura, T. (2008). AML1 mutations induced MDS and MDS/AML in a mouse BMT model. Blood *111*, 4297–4308.

Weinblatt, M.E., Scimeca, P., James-Herry, A., Sahdev, I., and Kochen, J. (1995). Transformation of congenital neutropenia into monosomy 7 and acute nonlymphoblastic leukemia in a child treated with granulocyte colony-stimulating factor. J. Pediatr. *126*, 263–265.

Wolff, L., Garin, M.T., Koller, R., Bies, J., Liao, W., Malumbres, M., Tessarollo, L., Powell, D., and Perella, C. (2003). Hypermethylation of the Ink4b locus in murine myeloid leukemia and increased susceptibility to leukemia in p15(Ink4b)-deficient mice. Oncogene *22*, 9265–9274.

Yamashita, N., Osato, M., Huang, L., Yanagida, M., Kogan, S.C., Iwasaki, M., Nakamura, T., Shigesada, K., Asou, N., and Ito, Y. (2005). Haploinsufficiency of Runx1/AML1 promotes myeloid features and leukaemogenesis in BXH2 mice. Br. J. Haematol. *131*, 495–507.